PAPER

Efficient quantum cutting in hexagonal NaGdF$_4$:Eu^{3+} nanorods†

Pushpal Ghosh, Sifu Tang and Anja-Verena Mudring*

An ionic liquid (IL) assisted solvothermal method is employed to prepare single phase, oxygen free, hexagonal NaGdF$_4$:Eu^{3+} (2 mol%) nanorods with a visible quantum efficiency of 187%. In contrast, for mixed materials containing cubic and hexagonal NaGdF$_4$:Eu^{3+}, the quantum efficiency is much less (127%). Thus, synthesis parameters have to be carefully chosen in order to get the high performance hexagonal material. Not only the influence of the IL but also of the Gd : F ratio during synthesis as well as the temperature were studied. It is found that the IL stabilizes the formation of hexagonal NaGdF$_4$:Eu^{3+}, likewise a fluoride excess (Gd : F = 1 : 8) and elevated reaction temperatures (200 °C).

Introduction

Energy efficient lighting is the need of the hour as nearly nineteen percent of global electricity generation is consumed for lighting—which is more than produced by hydro or nuclear stations and about the same as that produced from natural gas.[1] Incandescent lamps, which are so far widely used, suffer from a pour luminous efficiency as most of the energy is converted to heat, and are replaced more and more by environmentally benign light sources such as light emitting diodes (LEDs) and compact fluorescent lamps (CFLs). Especially CFLs are extensively used as they consume less energy and have a longer rated life. But like all fluorescent lamps, CFLs also contain mercury which complicates their disposal and adds substantial health risks and environmental issues during manufacturing. A possible alternative, in which Hg is replaced by an environmentally safe noble gas like Xe, has several advantages like immediate start, essential for special applications like lamps in facsimile, copying machines and car brake lights. However, the discharge efficiency of Xe is less compared to Hg. In addition, conversion of the yet shorter wavelength radiation to visible light results in an even larger energy loss compared to Hg based CFLs. In order to make Xe based CFLs competitive, a quantum yield of the used phosphor larger than 100% needs to be achieved.[2] In 1974, a photon cascade emission converting VUV radiation into 405 nm and 480 nm photons with a visible quantum efficiency of 140% was reported.[3] Some time later a down conversion process was established based on a combination of two different rare-earth ions, Gd^{3+} and Eu^{3+}, where the excitation energy is transferred *via* a two step process from the quantum cutter

(Gd^{3+}) to the emitting ion (Eu^{3+}), resulting in the emission of two visible photons with a theoretical total quantum efficiency of 200%. Recently, GdF$_3$:Eu^{3+} nanoparticles of 145% quantum efficiency have been reported.[4] Despite the fact that ternary gadolinium fluorides such as NaGdF$_4$ belong to the most efficient optical materials used in photonics and biophotonics because of the low phonon energy, high refractive index and tunable crystal phase,[5] the quantum cutting abilities of nano-NaGdF$_4$:Eu have received no attention so far. The reason might be that the preparation of oxygen free materials on the nanoscale with high quantum yield close to the maximum theoretical limit is still a challenge.[6]

In the past few years, ionic liquids (ILs) as a neoteric and widely tunable class of compounds have attracted tremendous attention as "green" and "designer" solvents for organic catalysis and synthesis, for electrochemical applications and for f-element separation.[7] One of the important features of IL is their negligible vapor pressure which makes them environmentally benign solvents unlike other solvents typically used in synthesis. Despite their versatility, the use of ILs in inorganic synthesis is still in its infancy.[8] Like well known surface active substances, ILs can also form a protective electrostatic shell around nanoparticles (NPs) *via* the cation or anion to prevent agglomeration and to stabilize NPs. Besides this, ILs are "supramolecular" solvents due to extended hydrogen bond systems in the liquid state and can be used in the synthesis of extended ordered nanoscale structures or for morphology control through their templating effect. Shape and phase directing properties of RTILs were shown for the synthesis of TiO$_2$, ZnO, mesoporous silica, tellurium nanowires, CuO, Fe$_2$O$_3$, Bi$_2$S$_3$ and others.[9–11] In this article, we report the synthesis of oxygen free, single phase, hexagonal NaGdF$_4$:Eu^{3+} (2 mol%) nanorods of high quantum efficiency by employing an IL (C$_2$mimBr = 1-ethyl-3-methyl imidazolium bromide) assisted solvothermal method starting from sodium chloride and

lanthanide nitrates. Judicious choice of synthesis parameters is used to get the desired nanocrystals.

Experimentals

1-Ethyl-3methylimidazolium bromide (C₂mimBr)

Modifying a literature procedure,[12] 58 ml of ethyl bromide (0.79 mol, Sigma Aldrich 98%) and 48 ml of *N*-methyl imidazole (0.607 mol, Sigma Aldrich 99%) were refluxed under inert gas (Ar) atmosphere at 40 °C for 3 hours in a round bottom flask (250 ml). After cooling to room temperature, ethyl acetate was added and the product crashed out of the solution. After filtration the crude product was washed with ethyl acetate and dried under vacuum at 25 °C for 10 hours to give a white solid.[12]

NaGdF₄:Eu³⁺ nanorods

In a typical synthesis, 3 ml (0.2 M) NaCl (J. T. Baker), 3 ml (0.2 M) Gd(NO₃)₃ (Alfa Aesar) in water and the required amount of an aqueous solution of Eu(NO₃)₃ (Alfa Aesar) to give NaGdF₄:2 mol % EuF₃ were added to 18 ml ethanol containing 6 ml 5 wt% C₂mimBr solution. To the well stirred solution, the appropriate amount of an aqueous NH₄F (Sigma Aldrich) solution was added producing a Gd³⁺/F⁻ ratio of 1 : 4 and 1 : 8, respectively. The mixture was poured into a Teflon lined autoclave (Parr Instruments, Moline, Illinois, USA) and subsequently heated at 200 °C for 5 hours. In another experiment the reaction temperature was changed to 150 °C keeping the other reaction parameters constant ($n(\text{Gd}^{3+})/n(\text{F}^-) = 1 : 8$, $t = 5$ h). Finally experiments were carried out keeping all reaction parameters the same but omitting the addition of C₂mimBr. The obtained nanocrystals were collected by centrifugation, washed several times with methanol, ethanol and acetone and dried in an oven at 80 °C.

Charaterization

PXRD (powder X-ray diffraction) measurements were carried out on a Huber G70 diffractometer (Rimsting, Germany) using MoKα radiation ($\lambda = 0.07107$ nm). Rietveld refinements of PXRD data were carried out with FullProf.[13] TEM (transmission electron microscopy; FEI Tecnai F20 field emission gun TEM, Philips Electron Optics, Holland) was used to map the shape, size and lattice structure of the nanocrystals dispersed on a carbon coated copper grid from acetone solution. Morphological characterization was also carried out by a JEOL, JSM-6700F FESEM (Japan). The excitation, emission spectra and decay time of all samples were recorded on a Fluorolog 3 (Horiba Jobin Yvon, Germany) luminescence spectrometer equipped with steady and pulsed Xe lamps for sample excitation and a photomultiplier for signal detection. All measurements were performed at room and liquid nitrogen temperature. Excitation and emission spectra using high energy synchrotron radiation were taken at the beamline I (SUPERLUMI) of the Doris III storage ring at HASYLAB, Deutsches Elektronen Synchrotron (DESY) in Hamburg, Germany.[14] Infrared spectra of powders (FTIR) were recorded in the range 400–4000 cm⁻¹ on an Alpha FTIR spectrometer (Bruker Optics, in ATR mode with a diamond crystal). ¹H NMR was measured on a Bruker DPX-200 (200 MHz) (Karlsruhe, Deutschland).

Results and discussion

Solvothermal conversion of sodium chloride and lanthanide nitrates in ethanol/water yielded in all cases nanosized NaGdF₄:Eu³⁺ (2 mol%). Fourier transformed infrared (FTIR) spectra (ESI†, Fig. S1) of the samples prepared with C₂mimBr (1-ethyl-3-methyl imidazolium bromide) show no imidazole ring skeleton stretching vibration bands or stretching vibration of the C(2)–H in the imidazole ring, suggesting complete removal of ionic liquid. The absence of stretching or bending vibrational bands for –OH in the FTIR spectra also suggests that the as prepared sample is free from water and hydroxide contamination.

To further analyze the samples, especially with respect to phase identity and purity, PXRD investigations were carried out. NaGdF₄ is known to crystallize in two different phases. The thermodynamically stable hexagonal phase features three cationic sites.[15] Herein the site 1*a*, occupied by Gd³⁺, and 1*f*, which is occupied statistically by ½ Na⁺ and ½ Gd³⁺, exhibit a nine-fold coordination by fluoride (ESI†, Scheme S1).[15,16] In contrast, the structure of cubic NaGdF₄ is related to the fluorite type of structure where the Ca²⁺ sites are randomly occupied by Na⁺ and Gd³⁺. This high temperature phase exhibits an appreciable phase width on the GdF₃ rich side of the phase diagram.[17]

Pure, highly crystalline hexagonal NaGdF₄:Eu³⁺ is obtained in the presence of C₂mimBr at a reaction temperature of 200 °C if a two-fold stoichiometric excess of F⁻ with respect to Gd³⁺ is used (Fig. 1, top). In contrast, at 200 °C a mixture of cubic and hexagonal NaGdF₄:Eu³⁺ is obtained if, for NaGdF₄, the required stoichiometric ratio of Gd³⁺/F⁻ = 1 : 4 is chosen. Rietveld refinement yielded a phase ratio of 38.4(4) : 61.6(5) for the cubic : hexagonal material. This observation is in agreement with earlier reports that show that at lower Gd³⁺/F⁻ ratio the formation of cubic NaGdF₄ is favoured.[16,17] Similarly with lower reaction temperatures the precipitation of the less thermodynamically stable cubic phase should become more likely according to Ostwald's step rule. Thus, when keeping the Gd³⁺/F⁻ ratio 1 : 8 but lowering the synthesis temperature to 150 °C a mixture consisting of 20.9(3)% cubic and 79.1(7)% hexagonal NaGdF₄:Eu³⁺ (ESI†, Fig. S2) forms. The reaction
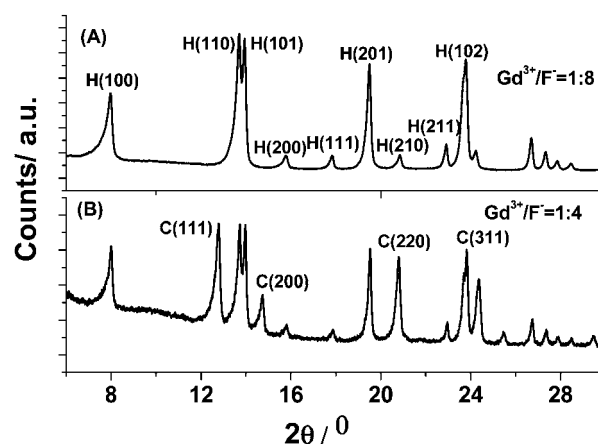

Fig. 1 PXRD pattern of NaGdF₄:Eu³⁺ nanocrystals prepared with different Gd³⁺/F⁻ ratios at 200 °C. At a Gd³⁺/F⁻ ratio of 1 : 8 (top) pure hexagonal NaGdF₄:Eu is obtained; whereas at a Gd³⁺/F⁻ ration of 1 : 4, a mixture of cubic and hexagonal NaGdF₄ forms.

conditions apparently do not allow for a full conversion of the cubic material to the thermodynamically stable hexagonal one. If no IL is used at all at 150 °C predominately cubic materials are formed (91.4(9)%) indicating a strong influence of the IL on the stabilization of the hexagonal phase at low reaction temperatures. Pure hexagonal $NaGdF_4$:Eu^{3+} (100(1)%) is obtained without IL at 200 °C (ESI†, Fig. S2).
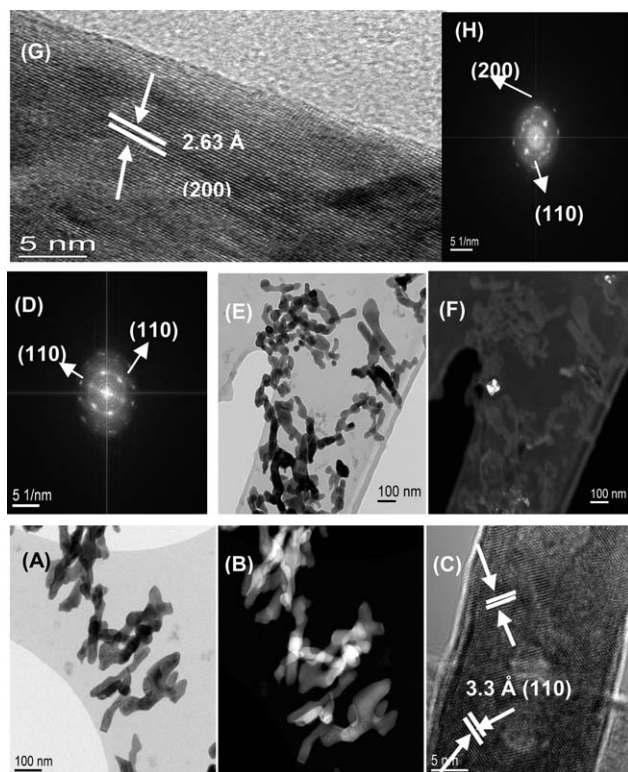
Fig. 2A shows the low magnification TEM image of $NaGdF_4$ nanocrystals prepared at 200 °C in the presence of C_2mimBr. Nanorods of an average diameter of 20 nm and an aspect ratio of 7–8.5 are obtained which is well confirmed by the HAADF-STEM images (Fig. 2B). The measured lattice spacing from the HRTEM image (Fig. 2C) is 3.3 Å, which corresponds to the theoretical d-spacing value of the (110) plane of hexagonal $NaGdF_4$ and is further confirmed by FFT studies (Fig. 2D). Energy dispersive X-ray analysis (EDXA) confirmed the presence of proper elemental composition (ESI†, Fig. S3).

Fig. 2E shows the low magnification TEM image of the sample prepared under similar reaction conditions without IL. Though the hexagonal crystal phase prevails, the average diameter of the nanorod is higher (35–40 nm) and the aspect ratio (4–5) is lower compared to the nanocrystal prepared with IL. This shows that C_2mim^+ is able to interact with growth facets of the hexagonal $NaGdF_4$, thus blocking some growth faces leading to nanocrystals of lower diameter and higher aspect ratio. Besides this, mutual π-stacking of imidazole rings of the IL may also favour

rod like structures with higher aspect ratios.[9] SEM images confirm these observations (ESI†, Fig. S4). Fig. 2F shows the dark field images of the samples shown in Fig. 2E and the bright spot corresponds to the (100) plane which was measured from the selected area electron diffraction (SAED) pattern (ESI†, Fig. S5). Again the measured lattice spacing of the HRTEM image is 2.63 Å (Fig. 2G), which corresponds to the hexagonal (200) plane and is further confirmed by the FFT pattern (Fig. 2H).

The excitation spectra of 2 mol% Eu^{3+} doped $NaGdF_4$ nanorods crystallized in the hexagonal phase (Fig. 3A and C) were measured at room temperature and 77 K respectively. Monitoring the $^5D_0$–$^7F_2$ electric dipole transition of the Eu^{3+} ion at 615 nm the narrow transition lines of Gd^{3+}, centered at 272 nm ($^8S_{7/2}$–^6I_J) and 310 nm ($^8S_{7/2}$–^6P_J) together with the typical Eu^{3+} transitions, can be seen. In the vacuum-UV (VUV) excitation spectrum (ESI†, Fig. S7) the Eu^{3+}–F^- charge transfer (CT) band below 180 nm becomes apparent but, most importantly, no Eu^{3+}–O^{2-} CT band is observed (which would be expected around 230 nm).[16] This confirms the absence of oxygen impurities in the sample. This finding is also confirmed by PXRD and FTIR studies (ESI†, Fig. S1). Fig. 3B shows a photoluminescence (PL) spectrum of $NaGdF_4$:Eu^{3+} nanocrystals recorded at RT under direct excitation of the $^7F_0$–$^5L_6$ transition of the Eu^{3+} ion (λ_{ex} = 393 nm). The prominent emission bands appear at 615 and 592 nm which originate from $^5D_0$–$^7F_2$ (electric dipole, e) and $^5D_0$–$^7F_1$ (magnetic dipole, m) transitions, respectively, in addition to transitions from higher ^5D_J (J = 1–3) levels to the ^7F manifold. The spectra are very similar to those already reported for Eu^{3+} doped $NaGdF_4$ nanocrystals.[16]

The hypersensitive forced electric dipole transition in the present case is more intense compared to the magnetic dipole indicating an acentric site symmetry of the Eu^{3+} ions in the host. For better understanding and quantification, we have calculated the asymmetry parameter using Judd–Ofelt theory.[18] The Ω_2-parameter gives information on the intensity and nature of the hypersensitive transition of the Eu^{3+} ion (for details see the ESI†). It is well known that a f–f transition arising from a forced electric dipole transition, which is parity forbidden, becomes

Fig. 2 (A–D) Low magnification TEM, high angle annular dark field (HAADF), scanning transmission electron microscopy (STEM) images, HRTEM and FFT pattern of $NaGdF_4$:Eu^{3+} nanocrystals prepared in the presence of IL. (E–H) TEM, dark field images, HRTEM and FFT pattern of hexagonal $NaGdF_4$:Eu^{3+} nanocrystals prepared in the absence of IL.
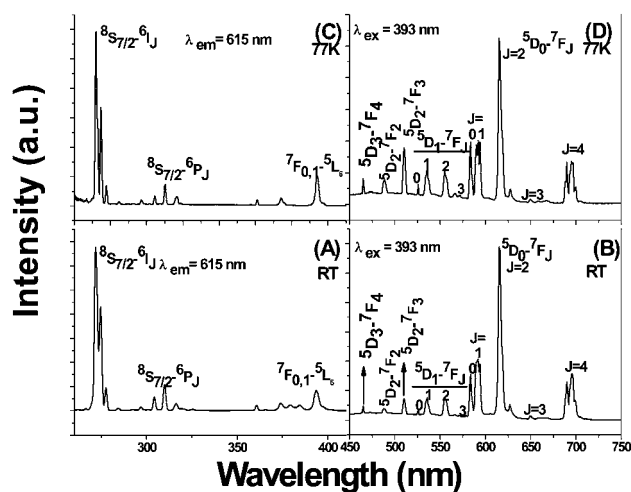
Fig. 3 Excitation (left) and emission (right) (PL) spectra of hexagonal $NaGdF_4$:Eu^{3+} nanocrystals measured at room temperature (RT, bottom) and 77 K (top).

partially allowed when the ion is situated at a low symmetry site. The higher Ω_2 (13.94×10^{-20} cm^2) value calculated for the pure hexagonal phase compared to the mixed phase (5.8×10^{-20} cm^2 and ESI†, Fig. S8) suggests that the Eu^{3+} ion resides in a highly asymmetric environment in the pure hexagonal NaGdF$_4$ lattice resulting in stronger optical transition probability and radiative emission. The intensity ratio $I(^5D_0 \rightarrow {}^7F_2)/I(^5D_0 \rightarrow {}^7F_1)$ of the electric dipole to magnetic dipole transition also serves as an effective spectroscopic probe of the site symmetry in which europium is situated. High values indicate the absence of a centre of inversion for the Eu^{3+} site, low values the presence.[19] However, there are some exceptions as observed for K$_5$Li$_2$LnF$_{10}$, in which Eu^{3+} occupies a site with C_s symmetry and the hypersensitive electric dipole transitions are weak.[19] In our case, for the pure hexagonal sample, an e/m ratio of 2.69 is determined whereas for the mixed cubic and hexagonal material it is 1.14.[16]

Fig. 3D represents the PL spectra recorded at 77 K under direct excitation. Interestingly, the transitions from the higher level such as $^5D_3$, $^5D_2$, and $^5D_1$ increases significantly compared to the sample measured at RT. The increased relative intensity from the higher energy transitions is due to a decreased multi-phonon relaxation between the higher ^5D levels at lower temperatures. Luminescence lifetime measurements also show that the $^5D_1$ lifetime increases by a factor of 2 (from 2.23 to 4.68 ms) if the temperature of measurement decreases from RT to 77 K whereas the $^5D_0$ life time increases only by 7% (from 9.17 to 9.82 ms) under the same conditions (ESI†, Fig. S11). To check this high lifetime value, we have calculated the radiative lifetime of the $^5D_0$ excited state of Eu^{3+}, directly from its corrected emission spectrum, without using Judd–Ofelt theory and according to the following equation:[20]

$$1/\tau_R = A_{MD,O}\eta^3(I_{tot}/I_{MD})$$

η is the measured refractive index of the solid sample, $A_{MD,O}$ is the spontaneous emission probability for the $^5D_0$–$^7F_1$ transition *in vacuo* (value is 14.65 s^{-1}), and I_{tot}/I_{MD} is the intensity ratio of the total area of the corrected Eu^{3+} emission spectrum to the area of $^5D_0$–$^7F_1$ band. The calculated radiative life time values of the $^5D_0$ state for the pure hexagonal sample measured at room temperature and low temperature are 8.8 and 9.1 ms, respectively, and match nicely with measured results.

The emission spectra of pure hexagonal NaGdF$_4$:Eu^{3+} recorded with high intensity VUV synchrotron radiation (202 and 305 nm) is depicted in Fig. 4. Upon excitation in the ^6G_J level, quantum cutting through a two step energy transfer takes place. In the first step, cross relaxation Gd^{3+} (^6G_J), Eu^{3+} ($^7F_0$) $\rightarrow$ Gd^{3+} (^6P_J), Eu^{3+} ($^5D_0$) yields one photon and, in the second step, energy is transferred from the ^6P_J level of Gd^{3+} to a higher energy level of Eu^{3+}, yielding a normal branching ratio for the different ^5D_J emission lines. As the first energy transfer step only gives emission from the $^5D_0$ level, significant increase of the relative intensity upon excitation in the ^6G_J level is expected if quantum cutting through a two step energy transfer process happens. When excited by 305 nm (^6P_J), a single energy transfer step to Eu^{3+} occurs with normal branching ratio (for an energy scheme see ESI†, Fig. S12). Comparing the PL spectra using beams of different incident wavelengths (202 and 305 nm), it is seen that the intensity of the $^5D_0$ emission line is substantially higher for excitation in

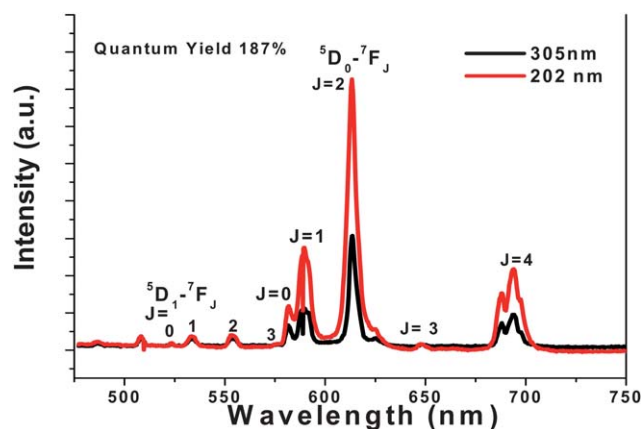**Fig. 4** Emission spectra of hexagonal NaGdF$_4$:Eu^{3+} (2 mol%) upon excitation in the ^6G_J levels of Gd^{3+} at 202 nm (red) and upon excitation in the ^6P_J levels of Gd^{3+} at 305 nm (black).

the ^6G_J levels than for excitation in the ^6P_J levels, confirming the occurrence of quantum cutting. The intensity ratio of $^5D_0/^5D_{1,2,3}$ was calculated both for the ^6G_J and ^6P_J level excitation and the efficiency of the cross relaxation step is determined[2] to be 87%. In consequence, a visible quantum efficiency of 187% (see the ESI†) is achieved which is close to the theoretical maximum value of 200%. In contrast, for the mixed phase, the quantum efficiency is much less (127%), compared to the pure hexagonal phase (Fig. 5).

We attribute this circumstance to the structural features of NaGdF$_4$. In hexagonal NaGdF$_4$ the lanthanide ions are surrounded in their second coordination sphere by a bicapped trigonal prism with two rather short ($\sim$363 pm) and six larger interatomic Ln–Ln distances ($\sim$393 pm). As Eu^{3+} ions are very close to the Gd^{3+} ions, the probability of energy transfer is large. In the cubic NaGdF$_4$ structure the lanthanide ions feature a cuboctahedron of lanthanide ions as the second coordination sphere. Although the coordination number is higher the interatomic distances ($\sim$383 pm) are also larger resulting in a substantially reduced interaction.
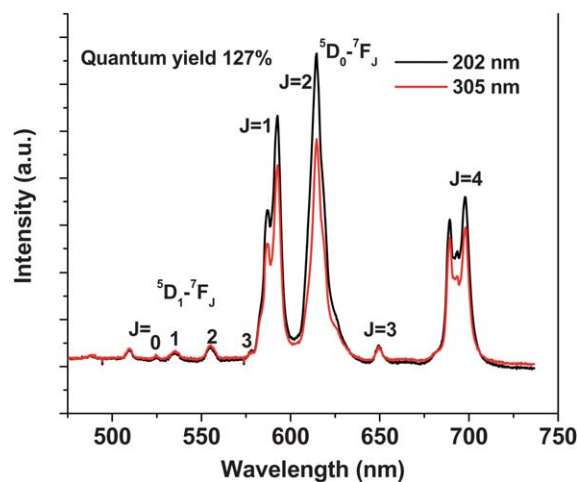

Fig. 5 Emission spectra of the mixed cubic/hexagonal phase NaGdF$_4$:Eu^{3+} (2 mol%) material prepared at Gd^{3+}/F$^-$ ratio 1 : 4, upon excitation in the ^6G_J levels of Gd^{3+} at 202 nm (black) and upon excitation in the ^6P_J levels of Gd^{3+} at 305 nm (red).

Conclusions

Ionic liquid assisted solvothermal synthesis allows for a fast and easy access to phase pure, hexagonal $NaGdF_4$:Eu^{3+} (2 mol%) with exceptionally good quantum cutting abilities. VUV spectroscopy reveals it to be as high as 187%. Most vital for such materials, this synthesis route allows us to obtain materials that are free from oxygen impurities as those would reduce the quantum cutting performance. Also mixed hexagonal/cubic materials have a reduced performance, e.g. a sample containing 38.4(4) mol% cubic $NaGdF_4$:Eu^{3+} yielded a quantum efficiency of only 127%. Thus, the reaction parameters have to be chosen carefully to obtain pure hexagonal $NaGdF_4$:Eu^{3+}. An excess of F^- during the synthesis (Gd : F = 1 : 8) favours the formation of hexagonal $NaGdF_4$:Eu^{3+} as well as slightly elevated reaction temperatures (200 °C vs. 150 °C). Most importantly, the presence of the ionic liquid additive, C_2mimBr, is mandatory as only in that case phase pure hexagonal material is obtained that shows the exceptionally high quantum yields.

Acknowledgements

Notes and references

1 http://news.bbc.co.uk/2/hi/science/nature/5128478.stm, accessed April 1st 2011.
2 R. T. Wegh, H. Donker, K. D. Oskam and A. Meijerink, Science, 1999, 283, 663.
3 (a) J. L. Sommerdijk, A. Bril and A. W. de Jager, J. Lumin., 1974, 8, 341; (b) W. W. Piper, J. A. DeLuca and F. S. Ham, J. Lumin., 1974, 8, 344.
4 C. Lorbeer, J. Cybinska and A.-V. Mudring, Chem. Commun., 2010, 46, 571.
5 (a) F. Wang, Y. Han, C. S. Lim, Y. Lu, J. Wang, J. Xu, H. Chen, C. Zhang, M. Hong and X. Liu, Nature, 2010, 463, 1062; (b) F. Wang, J. Wang and X. Liu, Angew. Chem., Int. Ed., 2010, 49, 7456; (c) Z.-L. Wang, J. H. Hao and H. L. W. Chan, J. Mater. Chem., 2010, 20, 3178; (d) K. A. Abel, J.-C. Boyer and F. C. J. M. Veggel, J. Am. Chem. Soc., 2009, 131, 14644; (e) R. Kumar, M. Nyk, T. Y. Ohulchanskyy, C. A. Flask and P. N. Prasad, Adv. Funct. Mater., 2009, 19, 853; (f) Y. Liu, D. Tu, H. Zhu, R. Li, W. Luo and X. Chen, Adv. Mater., 2010, 22, 3266; (g) E. V. D. Kolk, P. Dorenbos, K. Krämer, D. Biner and H. U. Güdel, Phys. Rev. B: Condens. Matter Mater. Phys., 2008, 77, 125110; (h) H.-X. Mai, Y.-W. Zhang, R. Si, Z.-G. Yan, L.-D. Sun, L.-P. You and C.-H. Yan, J. Am. Chem. Soc., 2006, 128,

6426; (i) F. Wang, X. Fan, M. Wang and Y. Zhang, Nanotechnology, 2007, 18, 025701; (j) C. Liu, J. Liu, S. Liu, B. Chen and J. Zhang, J. Lumin., 2007, 122–123, 970; (k) Y. I. Park, J. H. Kim, K. T. Lee, K.-S. Jeon, H. B. Na, J. H. Yu, H. M. Kim, N. Lee, S. H. Choi, S.-I. Baik, H. Kim, S. P. Park, B.-J. Park, Y. W. Kim, S. H. Lee, S.-Y. Yoon, I. C. Song, W. K. Moon, Y. D. Suh and T. Hyeon, Adv. Mater., 2009, 21, 4467; (l) F. You, S. Huang, S. Liu and Y. Tao, J. Lumin., 2004, 110, 95; (m) J. H. Zeng, Z. H. Li, J. Su, R. Yan and Y. Li, Nanotechnology, 2006, 17, 3549.
6 M. M. Lezhnina, T. Jüstel, H. Kätker, D. U. Wiechert and U. H. Kynast, Adv. Funct. Mater., 2006, 16, 935.
7 (a) T. Welton, Chem. Rev., 1999, 99, 2071; (b) J. H. Davis, Jr, in ACS Symp. Ser. 818, ed. R. D. Rogers and K. R. Seddon, ACS, Washington, 2002, pp. 247–258; (c) A. Bösmann, G. Francio, E. Janssen, M. Solinas, W. Leitner and P. Wasserscheid, Angew. Chem., Int. Ed., 2001, 40, 2697.
8 (a) C. Zhang and J. Chen, Chem. Commun., 2010, 46, 592; (b) X. Liu, J. Zhao, Y. Sun, K. Song, Y. Yu, C. Du, X. Kong and H. Zhang, Chem. Commun., 2009, 6628.
9 (a) Y. Zhou and M. Antonietti, J. Am. Chem. Soc., 2003, 125, 14960; (b) W. Zheng, X. Liu, Z. Yan and L. Zhu, ACS Nano, 2009, 3, 115; (c) L. Wang, L. Chang, B. Zhao, Z. Yuan, G. Shao and W. Zheng, Inorg. Chem., 2008, 47, 1443.
10 (a) B. G. Trewyn, C. M. Whitman and V. S.-Y. Lin, Nano Lett., 2004, 4, 2139; (b) Y.-J. Zhu, W.-W. Wang, R.-J. Qi and X.-L. Hu, Angew. Chem., Int. Ed., 2004, 43, 1410.
11 (a) X. Xu, M. Zhang, J. Feng and M. Zhang, Mater. Lett., 2008, 62, 2787; (b) J. Jiang, S.-H. Yu, W.-T. Yao, H. Ge and G.-Z. Zhang, Chem. Mater., 2005, 17, 6094.
12 E. R. Parnham, A. M. Z. Slawin and R. E. Morris, J. Solid State Chem., 2007, 180, 49.
13 J. R. Carvajal, Phys. B, 1993, 192, 55.
14 (a) G. Zimmerer, Radiat. Meas., 2007, 42, 859; (b) G. Zimmerer, J. Lumin., 2006, 106/107, 1; (c) http://hasylab.desy.de/facilities/doris_iii/beamlines/i_superlumi/experimental_station/index_eng.html, accessed April 1st 2010.
15 (a) J. H. Burns, Inorg. Chem., 1965, 4, 881; (b) L. Wang and Y. Li, Chem. Commun., 2006, 2557.
16 (a) P. Ptacek, H. Schäfer, K. Kömpe and M. Haase, Adv. Funct. Mater., 2007, 17, 3843; (b) P. Ptacek, H. Schäfer, O. Zerzouf, K. Kömpe and M. Haase, Cryst. Growth Des., 2010, 10, 2434; (c) A. Mech, M. Karbowiak, L. Kepinski, A. Bednarkiewicz and W. Strek, J. Alloys Compd., 2004, 380, 315.
17 (a) A. Grzechnik, P. Bouvier, M. Mezouar, M. D. Mathews, A. K. Tyagi and J. Köhler, J. Solid State Chem., 2002, 165, 159; (b) R. E. Thoma, H. Insley and G. M. Hebert, Inorg. Chem., 1966, 5, 1222; (c) P. Ghosh and A. Patra, J. Phys. Chem. C, 2008, 112, 3223.
18 (a) B. R. Judd, Phys. Rev., 1962, 127, 750; (b) G. S. Ofelt, J. Chem. Phys., 1962, 37, 511.
19 (a) A. Parma, I. Freris, P. Riello, F. Enrichi, D. Cristofori and A. Benedetti, J. Lumin., 2010, 130, 2429; (b) P. Solarz and W. Ryba-Romanowski, Phys. Rev. B: Condens. Matter Mater. Phys., 2005, 72, 075105; (c) W. Ryba-Romanowski, P. Solarz, G. Domimiak-Dzik and M. Gusowski, Opt. Mater., 2006, 28, 77.
20 (a) G. Blasse and B. C. Grabmaier, Luminescent Materials, Springer Verlag, NewYork, 1994; (b) M. H. V. Werts, R. T. F. Jukes and J. W. Verhoeven, Phys. Chem. Chem. Phys., 2002, 4, 1542.